

Super-resolving refractive index measurements with even coherent-state sources and parity detection

Qiang Wang(王强), Xiaohao Yang(杨晓豪), Fu Song(宋甫), and Lili Hao(郝利丽)
Citation: Chin. Phys. B, 2025, 34 (**12**): 124202. DOI: 10.1088/1674-1056/ade8de
http://cpb.iphy.ac.cn; http://iopscience.iop.org/cpb

What follows is a list of articles you may be interested in

Color Fourier single-pixel imaging with random color filter array

Jialiang Chen(陈佳亮), Wei Zhu(朱维), Le Wang(王乐), and Shengmei Zhao(赵生妹)
Chin. Phys. B, 2025, 34 (**9**): 094210. DOI: 10.1088/1674-1056/adf1e9

Strain modulation of second harmonic generation in new tetrahedral transition metal dichalcogenide monolayers

Hu Chen(陈虎), Shi-Qi Li(李仕琪), Yuqing Wu(吴雨晴), Xiaozhendong Bao(鲍晓振东), Zhijie Lei(雷志杰), Hongsheng Liu(柳洪盛), Yuee Xie(谢月娥), Junfeng Gao(高峻峰), Yuanping Chen(陈元平), and Xiaohong Yan(颜晓红)
Chin. Phys. B, 2025, 34 (**8**): 084206. DOI: 10.1088/1674-1056/addaa3

Quasi-two-dimensional isotropic laser cooling of atoms for quantum sensing

Xiao Zhang(张孝), Yi Song(宋屹), Yuan Sun(孙远), and Liang Liu(刘亮)
Chin. Phys. B, 2025, 34 (**8**): 084202. DOI: 10.1088/1674-1056/add4f7

Cascaded tilted fiber Bragg grating for enhanced refractive index sensing

Biqiang Jiang(姜碧强), Zhixuan Bi(毕芷瑄), Shouheng Wang(王守恒), Teli Xi(席特立), Kaiming Zhou, Lin Zhang, Jianlin Zhao(赵建林)
Chin. Phys. B, 2018, 27 (**11**): 114220. DOI: 10.1088/1674-1056/27/11/114220

Estimation of photon counting statistics with imperfect detectors

Xiao-Chuan Han(韩晓川), Dong-Wei Zhuang(庄东炜), Yu-Xuan Li(李雨轩), Jun-Feng Song(宋俊峰), Yong-Sheng Zhang(张永生)
Chin. Phys. B, 2018, 27 (**7**): 074208. DOI: 10.1088/1674-1056/27/7/074208

Super-resolving refractive index measurements with even coherent-state sources and parity detection

Qiang Wang(王强), Xiaohao Yang(杨晓豪)†, Fu Song(宋甫), and Lili Hao(郝利丽)

School of Physics and Electronic Engineering, Northeast Petroleum University, Daqing 163318, *China*

(Received 18 March 2025; revised manuscript received 6 June 2025; accepted manuscript online 27 June 2025)

High-precision refractive index measurement has become a research hotspot in recent years. However, traditional refractive index measurement often adopts intensity detection, whose performance is restricted by the classical detection limit and is thus hard to improve further. In order to break through this limitation, we propose a quantum-enhanced refractive index sensing scheme utilizing even-coherent-state sources in combination with parity detection. In this paper, we analyze the detection performance of the proposed system. Due to the inevitable photon loss in practical applications, the effects of photon loss on resolution and sensitivity are also investigated. Numerical results show that the resolution of the proposed strategy breaks through the Rayleigh limit and achieves super-resolving refractive index measurement. Relative to existing coherent-state schemes, our strategy leads to a twofold resolution improvement. Furthermore, the physical origins of the super-resolution are analyzed.

Keywords: refractive index measurement, even coherent state, parity photon counting, detection, super-resolution

PACS: 42.50.–p, 42.50.St

DOI: 10.1088/1674-1056/ade8de **CSTR:** 32038.14.CPB.ade8de

1. Introduction

The refractive index (RI) is a key optical parameter defined as the ratio of the speed of light in a vacuum to that in a medium.[1] As a fundamental property that characterizes material characteristics, the RI plays a pivotal role in a wide range of scientific and industrial fields, such as biology,[2–5] medicine,[6] petrochemicals,[7,8] and environmental science.[9,10] The extensive use of RI measurements arises from their capability to provide essential information about samples via nondestructive testing. By measuring the RI, various sample properties can be determined, including liquid concentration, food quality, and so on. Given its broad applicability and significance in material characterization, advancing accurate and sensitive RI measurement techniques has become a major research focus.

In the early stages of high-precision RI measurement, most methods were based on wave optics principles and implemented using optical interferometers. Typical optical interferometers include Fabry–Pérot interferometers,[11–13] Michelson interferometers,[14–16] and Mach–Zehnder interferometers (MZIs).[17–19] These instruments utilize optical interference phenomena to transform RI variations into optical path length differences, enabling high-precision measurements based on the detection of interference fringe displacement or phase shifts. Despite their high measurement accuracy, optical interferometers face challenges in practical applications due to their relatively large physical dimensions and susceptibility to environmental disturbances. In parallel, RI sensors based on surface plasmon resonance (SPR) have emerged as a major research focus. In contrast to interference-based approaches, SPR sensors demonstrate remarkable competitiveness across multiple fields due to their unique sensing mechanism.[20–22] Recent advances in optical fiber micro/nanofabrication techniques have enabled the successful integration of both interferometric structures and SPR sensing mechanisms within optical fibers. This innovation has led to the development of fiber-optic RI sensors that combine high sensitivity with electromagnetic interference immunity, miniaturization, and low optical loss,[23] establishing them as a predominant research direction in this field.[24] Pengcheng Chen *et al.*[11] proposed a compact RI sensor based on a Fabry–Pérot interferometer, which was spliced to a single-mode fiber by a small section of thin-core fiber and achieved an average sensitivity of 240 dB/refractive index unit (RIU) over a wide RI range of 1.3326–1.4305. Jin Wang *et al.*[14] proposed an in-line optical fiber RI sensor based on a Michelson interferometer, which was fused and spliced with a single-mode optical fiber and hollow-core silicon tubes; it achieved a sensitivity of 8.1498 rad/RIU in the RI range of 1.331–1.387. Jing Zhang *et al.*[17] proposed an all-fiber RI sensor based on an MZI which was spliced from coreless few-mode fibers; it achieved a maximum sensitivity of up to 25.29 nm/RIU in RI measurement.

The traditional RI measurement techniques based on wave optics mentioned above typically rely on interferometric spectrometers to detect wavelength shifts or intensity variations in interference fringes for RI determination. Spectrome-

†Corresponding author. E-mail: yangxiaohao0508@163.com

© 2025 Chinese Physical Society and IOP Publishing Ltd. All rights, including for text and data mining, AI training, and similar technologies, are reserved.

ters measure signal intensity using an optical power meter, analyze the change of fringe numbers, record the corresponding optical path difference, and then calculate the wavelength of the signal light. Therefore, intensity detection (ID) is still their underlying fundamental principle. However, the performance of these intensity-based methods is fundamentally constrained by the Rayleigh diffraction limit (RDL)[25] and shot noise limit (SNL),[26] and faces challenges for further performance enhancement. Recent developments in quantum optics have provided novel approaches that can overcome these limitations. Since the pioneering work by Boto *et al.*,[27] the utilization of quantum phenomena and detection methods has demonstrated the potential to significantly improve interferometric sensing performance. This quantum-enhanced approach promises to surpass classical detection limits and achieve super-resolution RI measurements.

In this paper, we propose a scheme for achieving super-resolution RI measurement using even coherent superposition state (ECSS) sources and a parity detection (PD) strategy, in addition to comprehensive theoretical derivations and numerical analyses. The results show that the sensitivity of even coherent state (CS) sources with PD matches the SNL, while their resolution significantly surpasses the RDL and enables super-resolution RI measurements. Compared with the CS scheme, the ECSS scheme has twice as much resolution in lossless cases. Even in lossy environments, the ECSS scheme still has certain advantages. In the conclusions, we explain the nature of parity-detection super-resolution and even-coherent-state super-resolution.

2. Principle

The RI measurement scheme with even CS sources and PD is realized by a modified MZI, which works as shown in Fig. 1. The even CS $|\mathrm{BCSS}\rangle = N_\mathrm{e}\left(|\mathrm{i}\alpha\rangle + |-\mathrm{i}\alpha\rangle\right)$ and the vacuum state $|0\rangle$ are injected into ports a and b of the MZI, respectively, and interfere at the first 50–50 beam splitter, BS1. Path b passes through the RI shifter (RIS) labeled RIS(n), which produces a phase shift of $\varphi = k(n-1)l$, where k is the wave number of the incident light and l is the sample length in the direction of beam propagation. The two beams interfere at BS2 after being reflected by mirrors M and attenuated by the virtual beam splitter B(T). The interference signals are acquired at the output port, and postprocessing operations are performed. Different detection strategies are adopted to estimate the RI of the sample, and the detection performance of the system is analyzed.

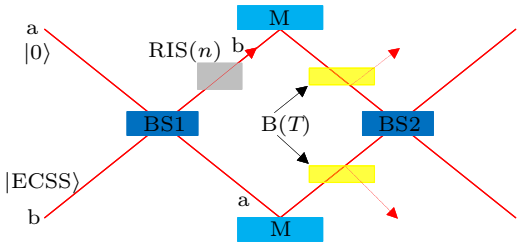


Fig. 1. Schematic of the super-resolution RI measurement with ECSS and PD. BS: 50–50 beam splitter; RIS: RI shifter; M: mirror; B(T): virtual beam splitter.

3. Methods

3.1. Intensity detection

The even CS beam $|\mathrm{BCSS}\rangle = N_\mathrm{e}\left(|\mathrm{i}\alpha\rangle + |-\mathrm{i}\alpha\rangle\right)$ and the vacuum state beam $|0\rangle$ are inputs to the MZI, where $N_\mathrm{e} = 1/\sqrt{2\left[1+\exp\left(-2N\right)\right]}$ is the normalized factor and $N = |\alpha|^2$ is the average number of photons in CS. The output state after BS1 can be expressed as

$$\psi_1 = N_\mathrm{e}\left(\left|\frac{\alpha}{2}, -\frac{\alpha}{2}\right\rangle + \left|-\frac{\alpha}{\sqrt{2}}, \frac{\alpha}{\sqrt{2}}\right\rangle\right). \tag{1}$$

After the beam has passed through RIS(n) and two virtual beam splitters B(T), the state can be further expressed as

$$\begin{aligned}\psi_2 = N_\mathrm{e}\Bigg(&\left|\frac{\sqrt{T}\alpha}{\sqrt{2}}, \frac{\sqrt{T}\alpha\exp[\mathrm{i}k(n-1)l]}{\sqrt{2}}\right\rangle \\ &+\left|-\frac{\sqrt{T}\alpha}{\sqrt{2}}, \frac{\sqrt{T}\alpha\exp[\mathrm{i}k(n-1)l]}{\sqrt{2}}\right\rangle\Bigg).\end{aligned} \tag{2}$$

The beams corresponding to the two paths interfere again at the second beam splitter BS2, and the output state is obtained from

$$\begin{aligned}\psi_\mathrm{out} = N_\mathrm{e}\big(&\left|\left(\mathrm{e}^{\mathrm{i}k(n-1)l}+1\right)\left(\sqrt{T}\gamma, -\sqrt{T}\beta\right)\right\rangle \\ &+\left|\left(\mathrm{e}^{\mathrm{i}k(n-1)l}-1\right)\left(-\sqrt{T}\gamma, \sqrt{T}\beta\right)\right\rangle\big),\end{aligned} \tag{3}$$

where $\gamma = \alpha\sin\left[\pi l\left(n-1\right)/\lambda\right]$, $\beta = \alpha\cos\left[\pi l\left(n-1\right)/\lambda\right]$, and λ is the incident light wavelength. The output signal of the MZI is detected. The specific expression for the ID signal is

$$\left\langle\hat{I}\right\rangle = NT\tanh\left(N\right)\sin^2\left[\frac{\pi l}{\lambda}\left(n-1\right)\right]. \tag{4}$$

According to Eq. (4) and the Gaussian error propagation formula $\delta n_I = \sqrt{\left\langle\hat{I}^2\right\rangle - \left\langle\hat{I}\right\rangle^2}\Big/\left|\partial\left\langle\hat{I}\right\rangle/\partial n\right|$, the sensitivity of the ID signal is

$$\delta n_I = \sqrt{\frac{NT\sin^4\left[\frac{\pi l}{\lambda}\left(n-1\right)\right]\mathrm{sech}^2\left(N\right) + \sin^2\left[\frac{\pi l}{\lambda}\left(n-1\right)\right]\tanh\left(N\right)}{NT\left(\frac{\pi l}{\lambda}\right)^2\tanh^2\left(N\right)\sin^2\left[\frac{2\pi l}{\lambda}\left(n-1\right)\right]}}. \tag{5}$$

The RDL and SNL represent the best detection performance that can be achieved using a classical CS light source and traditional intensity measurement methods. As demonstrated in Ref. [28], RI measurements using coherent-state light sources with ID can achieve resolutions of up to λ/l (RDL), and sensitivities of up to $\lambda/(2\pi l\sqrt{TN})$ (SNL). The ID performance of the ECSS proposed in this chapter is the same as that of the CS scheme; that is, the resolution and optimal sensitivity of this scheme reach the RDL and the SNL, respectively. Theoretically, the traditional measurement methods are limited by this bottleneck. To overcome the classical limit in RI measurements, detection schemes must be revolutionized.

3.2. Parity detection

PD was originally proposed by Bollinger *et al.* in 1996[29] and later adopted for phase estimation by Gerry.[30] PD guarantees the best measurement of phase shift in optical interferometers in a variety of nonclassical input states. Compared with classical ID, PD can break through the classical resolution limitations and sensitivity limitations and realize super-resolution and super-sensitivity measurements. The parity operator $\hat{\Pi} = \mathrm{e}^{\mathrm{i}\hat{N}\pi}$ is intimately related to the Wigner function, which can be expressed as the expectation value of the displaced parity operator.[31] For the input state $|\mathrm{ECSS}\rangle_{\mathrm{aa}}\langle\mathrm{ECSS}| \otimes |0\rangle_{\mathrm{bb}}\langle 0|$, the Wigner function can be expressed as

$$W_{\mathrm{in}}(\gamma,\beta) = W_{|\mathrm{ECSS}\rangle_{\mathrm{a}}}(\gamma)\, W_{|0\rangle_{\mathrm{b}}}(\beta), \tag{6}$$

where $W_{|\mathrm{ECSS}\rangle_{\mathrm{a}}}(\gamma)$ and $W_{|0\rangle_{\mathrm{b}}}(\beta)$ are the Wigner functions corresponding to the even CS and vacuum states, respectively. We make the following replacements in $W_{\mathrm{in}}(\gamma,\beta)$:

$$\gamma \to \gamma_1 = \gamma\cos\left[\frac{\pi l}{\lambda}(n-1)\right] + \beta\sin\left[\frac{\pi l}{\lambda}(n-1)\right], \tag{7}$$

$$\beta \to \beta_1 = -\gamma\sin\left[\frac{\pi l}{\lambda}(n-1)\right] + \beta\cos\left[\frac{\pi l}{\lambda}(n-1)\right], \tag{8}$$

and the Wigner function for the input state is then transformed as follows:

$$W_{\mathrm{out}}(\gamma,\beta) = W_{\mathrm{in}}(\gamma_1,\beta_1). \tag{9}$$

Finally, the average value of the parity operator at the output port can be expressed as

$$\langle\hat{\Pi}\rangle = \frac{\pi}{2}\int_{-\infty}^{+\infty} W_{\mathrm{out}}(0,\beta)\,\mathrm{d}^2\beta. \tag{10}$$

After considering the influence of photon loss, the specific expression for the PD signal is

$$\langle\hat{\Pi}\rangle = 2|N_{\mathrm{e}}|^2\left\{\mathrm{e}^{-2NT\sin^2\left[\frac{\pi l}{\lambda}(n-1)\right]} + \mathrm{e}^{-2NT\cos^2\left[\frac{\pi l}{\lambda}(n-1)\right]-2NR}\right\}, \tag{11}$$

where R represents the photon loss and $R = 1-T$.

According to Eq. (11) and the Gaussian error propagation formula, the sensitivity of the parity signals is

$$\delta n_{\mathrm{p}} = \sqrt{\frac{1-\left|4|N_{\mathrm{e}}|^4\left\{\mathrm{e}^{-2NT\sin^2\left[\frac{\pi l}{\lambda}(n-1)\right]} + \mathrm{e}^{-2NT\cos^2\left[\frac{\pi l}{\lambda}(n-1)\right]-2NR}\right\}^2\right|}{\left|4|N_{\mathrm{e}}|^2 NT\sin\left[\frac{\pi l}{\lambda}(n-1)\right]\frac{\pi l}{\lambda}\left\{\mathrm{e}^{-2NT\sin^2\left[\frac{\pi l}{\lambda}(n-1)\right]} + \mathrm{e}^{-2NT\cos^2\left[\frac{\pi l}{\lambda}(n-1)\right]-2NR}\right\}\right|^2}}. \tag{12}$$

4. The resolution and sensitivity of intensity detection and parity detection

Figures 2(a)–2(c) show the normalized ID and PD signals for photon numbers $N = 5$, 10, and 15, respectively, where $T = 1$, $l = 5.3$ mm, and $\lambda = 532$ nm. Figure 2 shows that PD has a narrower peak width, which indicates that PD has better resolution. With increasing N, the peak width of the intensity-detected signal does not change, while the peak width of the parity signal becomes narrower, indicating its excellent resolution. The reason for this characteristic is that the resolution of the intensity-detected signal is determined by $\sin^2\left[\frac{\pi l}{\lambda}(n-1)\right]$, which does not contain the photon number N, so its resolution is not affected by N, and N only affects its amplitude. However, the resolution of the PD is determined by $\exp\left\{-2NT\sin^2\left[\frac{\pi l}{\lambda}(n-1)\right]\right\} + \exp\left\{-2NT\cos^2\left[\frac{\pi l}{\lambda}(n-1)\right]-2NR\right\}$, which, in the small angle limit, is effectively $\exp\left[-2NT(\pi l/\lambda)^2(n-1)^2\right] + \exp(-2NT)$. Its shape conforms to the characteristics of the Gaussian distribution function $f(x) = \exp\left[-\frac{(x-\mu)^2}{2\sigma^2}\right]$; thus, the peak width can be expressed as $\sigma = \lambda/(2\pi l\sqrt{TN})$, while σ becomes smaller with increasing N. This indicates a narrow peak and results in excellent resolution. The result of $\sigma = \lambda/(2\pi l\sqrt{TN})$ is the same as that of the CS scheme. From a mathematical point of view, the parity signal for an even CS source contains two Gaussian distribution terms, while the CS parity signal contains only a single Gaussian term; therefore, the number of peaks of the even CS parity signal is twice that of the CS parity signal. This confirms the doubled resolution. In order to show the doubled super-resolution of the even CSs more intuitively, the resolution of the signal is expressed in terms of the full width at half maximum (FWHM), and then the average resolution of the signal can further be expressed as $\overline{\delta\chi} = \frac{\mathrm{FWHM}}{1+\exp(-2NR)}$. Figure 2(d) demonstrates the influence of the photon number N on the resolutions of ID and PD. As the photon number N increases, the resolution available via

ID remains constant, while the resolution available via PD becomes progressively better and is always superior to that obtained via ID. Simultaneously, the PD available via ECSS represents about a twofold resolution improvement compared to the resolution available via CS. All of the above indicates that the scheme using ECSS and PD surpasses the RDL.

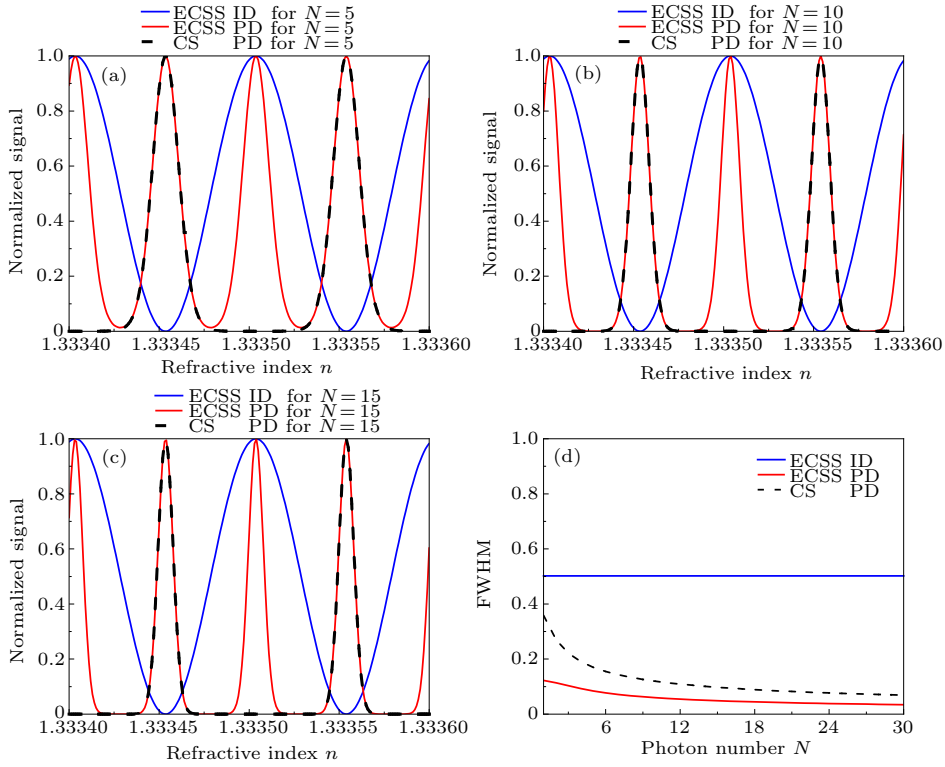


Fig. 2. Output signals obtained using ID and PD for $T = 1$, $\lambda = 532$ nm, and $l = 5.3$ mm. (a) $N = 5$, (b) $N = 10$, (c) $N = 15$. The horizontal axis represents the RI n, and the vertical axis represents the normalized signal. The blue solid line, red solid line, and black dashed line represent the signals of ID for ECSS, PD for ECSS, and PD for CS, respectively. (d) Variation of the resolutions of ID and PD with photon number N. The horizontal axis represents the photon number N, and the vertical axis represents the FWHM.

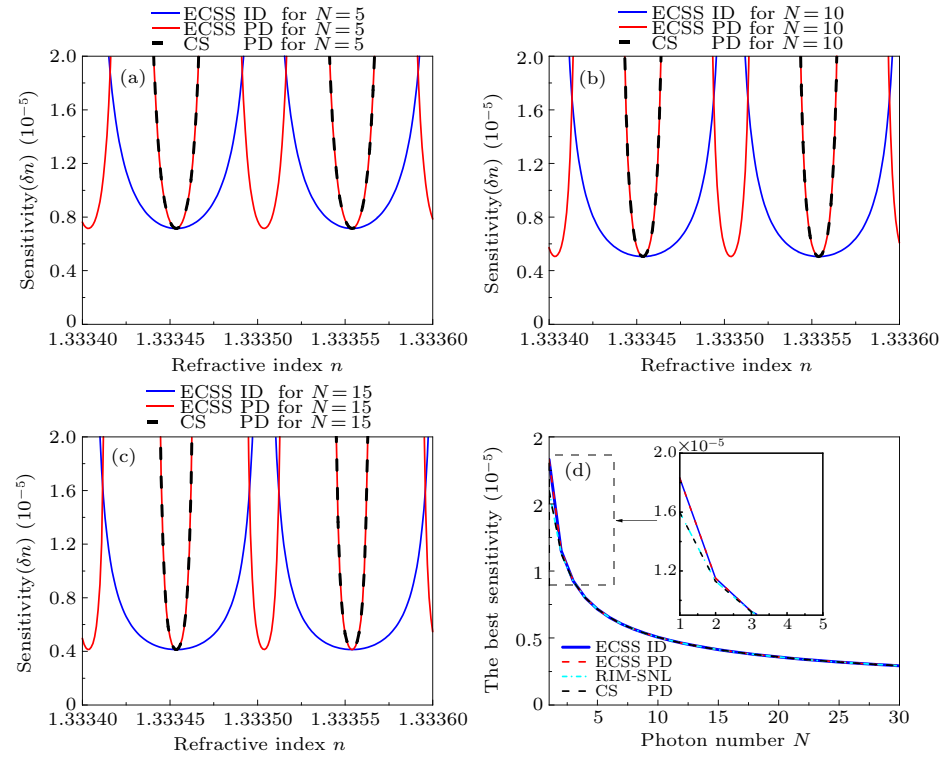


Fig. 3. The sensitivities of ID and PD for $T = 1$, $\lambda = 532$ nm, and $l = 5.3$ mm. (a) $N = 5$, (b) $N = 10$, (c) $N = 15$. The horizontal axis represents the RI n, and the vertical axis represents the sensitivity. The blue solid line, red solid line, and black dashed line indicate the sensitivities of ID for ECSS, PD for ECSS, and PD for CS, respectively. (d) Variation of the best sensitivity of ID and PD with photon number N. The horizontal axis represents the photon number N, and the vertical axis represents the best sensitivity.

Their sensitivities are depicted in Fig. 3. Figures 3(a)–3(c) show the sensitivity of ID and PD for photon numbers $N = 5$, 10, and 15, respectively, where $T = 1$, $\lambda = 532$ nm, and $l = 5.3$ mm. It is clear from Fig. 3 that the best sensitivities for ID and PD are always the same and that all these best sensitivities can reach the SNL. Figure 3(d) demonstrates the influence of photon number N on the best sensitivities of ID and PD. Compared with CS sources using the PD scheme, when N is comparatively small, the best sensitivity value of the parity signal for ECSS is larger than that of CS, which means that the best sensitivity of ECSS is slightly poorer than that of the CS. After that, all the best sensitivities converge to the same level, and they all become better with increasing N. The above analyses show that all the best sensitivities of the two detection methods can reach the SNL except in the case of low photon numbers; thus, the PD scheme can realize super-resolution RI measurement based on the SNL.

5. The impact of photon loss on resolution and sensitivity

In practical applications, photon loss is unavoidable. Such loss is mainly due to absorption and diffraction by the medium.[32] Photon loss is simulated by the reflectance R. When loss exists, $T \neq 1$.

Figures 4(a)–4(c) show normalized ID signals and PD signals for transmissivities $T = 0.9$, 0.95, and 1, respectively, where $N = 10$, $\lambda = 532$ nm, and $l = 5.3$ mm. In Fig. 4, the peak width of the ID signal is not affected by T, which indicates that its resolution is unchanged. The peak width of the PD signal is influenced by T: its resolution deteriorates with increasing loss. At the same time, as loss increases, half of the signal peaks for PD are sharply reduced until they disappear, which indicates that the doubled super-resolution is lost. The reasons for these phenomena are that the signal of an even CS source with PD is determined by the exponential part $\exp\left\{-2NT\sin^2\left[\frac{\pi l(n-1)}{\lambda}\right]\right\} + \exp\left\{-2NT\cos^2\left[\frac{\pi l(n-1)}{\lambda}\right] - 2NR\right\}$, where half of the signal peaks are determined by the first part and the other half of the peaks are determined by the second term associated with photon loss. The amplitudes of the peaks relative to loss sharply decline (exponentially) when the loss increases slowly, and this is the root of the disappearing doubled super-resolution characteristic. Figure 4(d) demonstrates the effect of T on the resolutions obtained via ID and PD. As the loss increases, the resolution obtained via ID remains constant, while that obtained via PD becomes less effective, although it is still better than that obtained via ID. ECSS has significantly better resolution than CS in the lower-loss region; however, the resolution of ECSS remains the same as that of CS at higher loss values.

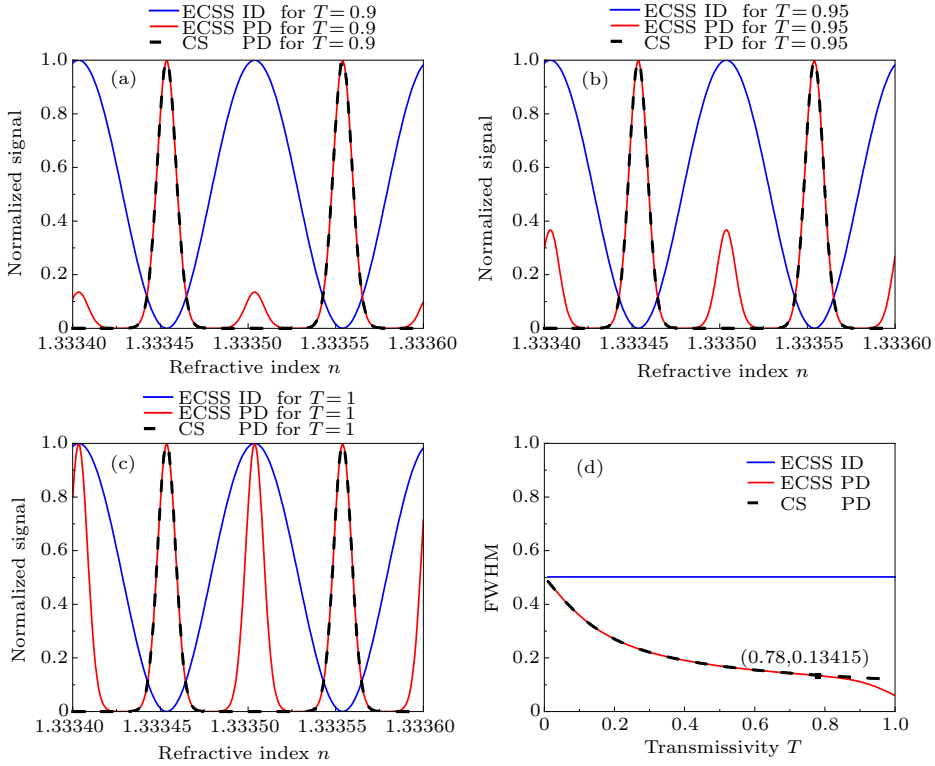


Fig. 4. Output signals obtained using ID and PD for $N = 10$, $\lambda = 532$ nm, and $l = 5.3$ mm. (a) $T = 0.9$, (b) $T = 0.95$, (c) $T = 1$. The horizontal axis represents the RI n, and the vertical axis represents the normalized signal. The blue solid line, red solid line, and black dashed line indicate the signals of ID for ECSS, PD for ECSS, and PD for CS, respectively. (d) Variation of the resolutions obtained using ID and PD with transmissivity T. The horizontal axis represents the transmissivity T, and the vertical axis represents the FWHM.

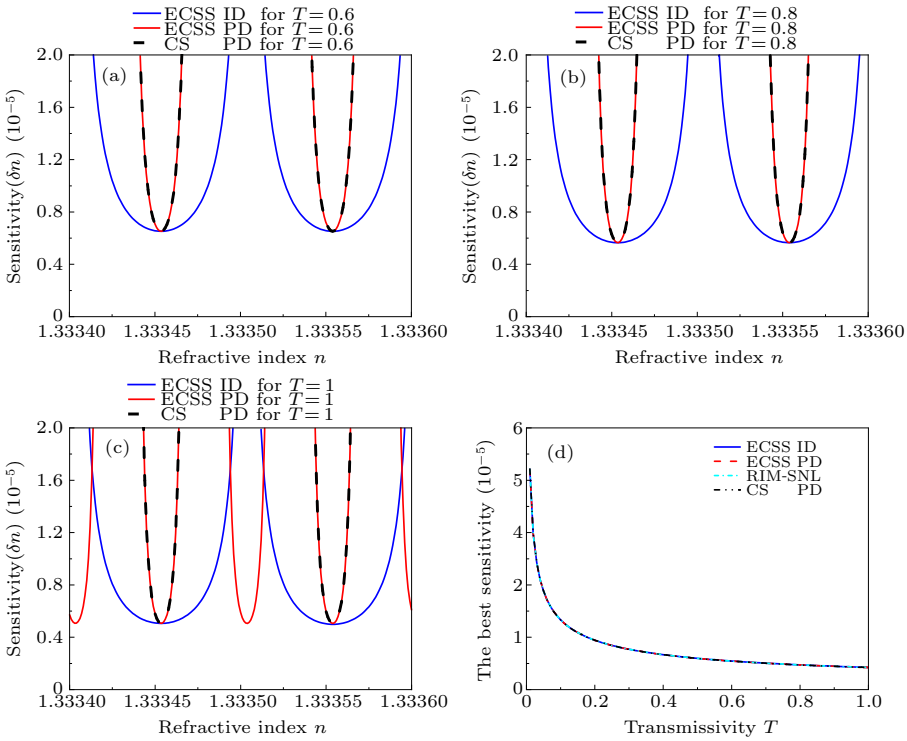


Fig. 5. The sensitivities of ID and PD for $N = 10$, $\lambda = 532$ nm, and $l = 5.3$ mm. (a) $T = 0.6$, (b) $T = 0.8$, (c) $T = 1$. The horizontal axis represents the RI n, and the vertical axis represents the sensitivity. The blue solid line, the red solid line, and the black dashed line indicate the sensitivities of ID for ECSS, PD for ECSS, and PD for CS, respectively. (d) Variation of the best sensitivities of ID and PD versus transmissivity T. The horizontal axis represents the transmissivity T, and the vertical axis represents the best sensitivity.

The effect of loss on sensitivity is analyzed next. Figures 5(a)–5(c) show the sensitivity of ID and PD for transmissivities $T = 0.6$, 0.8, and 1, respectively, where $N = 10$, $\lambda = 532$ nm, and $l = 5.3$ mm. It can be found from Fig. 5 that all the best sensitivities are always the same and deteriorate as the loss increases. Figure 5(d) demonstrates the impacts of the transmissivity T on the sensitivity of ID and PD. As T decays, the best sensitivity decreases; notably, this optimal sensitivity remains identical for both detection methods, and in both cases, the sensitivity reaches the SNL. For small T values, the best sensitivity curve demonstrates significant variation, while larger T values yield more gradual sensitivity changes. The above analysis shows that enhanced resolution and sensitivity can be achieved by increasing the incident photon number, while minimizing loss is crucial for maintaining measurement precision. The combined implementation of these strategies enables the simultaneous improvement of both resolution and sensitivity.

Loss is the most critical factor affecting detection performance, and suppressing its impact in practical applications remains a significant challenge. Quantum error correction schemes have emerged as effective technologies for mitigating losses, and substantial research is currently underway in this field. Related teams have investigated quantum state behavior and error correction techniques through MZIs, confirming the effectiveness of Shor's code in correcting both bit-flip and phase-flip errors. Their experiments demonstrate that the MZI framework achieves significant error correction for known coherent superposition states but still exhibits limitations in handling unknown superposition states. This provides critical directions for optimizing future quantum error correction technologies.[33] In addition to the above methods, preparing quantum states with strong robustness against photon loss is also a viable approach. Taking entangled states[34] and squeezed states[35] as examples, their unique physical properties can meet the requirements of loss resistance: if the influence of visibility is ignored, entangled states rely on quantum correlation redundancy to retain key information and maintain measurement accuracy in low-loss scenarios; squeezed states can still approach the quantum limit sensitivity in moderate-loss environments through noise component suppression mechanisms. In practical applications, it is necessary to adapt the corresponding state types according to specific scenarios and optimize error correction strategies in a coordinated manner to achieve a balance between loss suppression and performance improvement.

6. Discussion

So far, we have seen that the combined ECSS and PD scheme can offer superior super-resolution compared to the Rayleigh limit while maintaining sensitivity at the SNL. However, why is the resolution of ECSS double that of CS? And why does PD have narrower peaks than those of ID? What are the reasons for these phenomena? The even CS scheme uses

the same interferometer as the CS scheme,[36] so the performance improvement is independent of the interferometer used and depends mainly on the light source and detection method.

If the same interferometer and the same incident light sources are used, the improvement in detection performance can only be related to the detection strategy. ID is a method that can directly detect the optical intensity of the output signal, but its resolution is limited by the RDL and is difficult to improve. On the other hand, PD can be seen as projecting the output state onto an odd or even photon state to obtain the infinitely compressed state,[37] which is a photon state possessing a pure quantum nature that can be used to improve the signal resolution.[38] PD is similar to using the compressed state directly as an incident light source, omitting the cumbersome process of compressed state preparation.

In addition, if the same interferometer and the same detection method are used, then the resolution improvement can only be associated with the light sources. In an MZI, if a CS beam passes through the RIS(n), angular accumulation occurs. When a monochromatic beam of the ECSS passes through RIS(n), twice as much angular accumulation occurs, resulting in twice as much super-resolution, due to the fact that ECSS is a highly nonclassical quantum state formed by the superposition of two CSs with opposite phases.[39] The latter is equivalent to the passage of each of the two CSs of opposite phases through the RIS. It is the coherent superposition that produces the doubled resolution. This principle is somewhat similar to the $N00N$ state,[25] with the difference being that an alternative light source is used.

Both even coherent superposition states and $N00N$ states exhibit unique enhancement effects in quantum precision measurements, yet their underlying mechanisms differ fundamentally. The even coherent superposition state is formed through the linear superposition of two CSs, while the $N00N$ state represents a quantum entangled state that correlates and superposes the states of multiple photons. This entanglement enables the $N00N$ state to amplify phase variations by a factor of N, thereby achieving an N-fold improvement in resolution and a significant enhancement in sensitivity.[25] This performance markedly surpasses the twofold resolution enhancement characteristic of even coherent superposition states. However, while the entanglement properties of $N00N$ states confer superior detection capabilities, they also render the system highly susceptible to decoherence effects. Even minimal losses during transmission can lead to a sharp decline in measurement visibility, compromising the reliability of the results despite the state's exceptional precision.[40] In contrast, although even coherent superposition states offer comparatively lower measurement precision, their non-entangled nature ensures robust preservation of visibility, representing a distinct advantage in certain practical scenarios. In summary, both even coherent superposition states and $N00N$ states possess unique merits, and their relative advantages cannot be simplistically ranked. The choice between these states should be guided by specific application requirements, particularly considering factors such as system loss tolerance and the desired measurement precision.

The proposed scheme has demonstrated experimental feasibility.[41] while still presenting challenges in the preparation of large-photon-number even coherent superposition states and the implementation of PD. Currently, ECSS states can be prepared through two experimentally verified approaches: photon subtraction and addition techniques[42] or by injecting squeezed vacuum into a beam splitter followed by photon counting in the auxiliary mode.[43] While ECSS states with photon numbers up to $|\alpha|^2 = 3$ have been successfully prepared,[44] ongoing research aims to extend this capability to higher photon numbers.[45] PD, which requires one to distinguish the odd or even nature of photon numbers, is typically realized using photon-number-resolving detectors.[46,47] The current technological solution employs Geiger-mode avalanche photodiode arrays. However, these detectors exhibit fundamental limitations, as they can only register photon presence or absence rather than providing exact photon number resolution. Consequently, accurate measurements necessitate operation under weak light conditions, where photon statistics are obtained by accumulating detection events across the entire detector array. The practical implementation of PD is fundamentally constrained by the resolving capability of existing detection systems. Current detector technologies in this domain remain at a relatively early stage of development, indicating substantial potential for improvement in both detection efficiency and photon-number resolution capabilities.

7. Conclusions

This paper proposes a quantum-enhanced RI measurement scheme utilizing even CS sources combined with PD. Theoretical analysis demonstrates that the proposed method achieves SNL sensitivity while surpassing the RDL in resolution. Specifically, while conventional ID remains constrained by the RDL, the PD scheme exhibits significantly enhanced resolution under identical experimental conditions while maintaining comparable sensitivity. Compared to conventional CS approaches, the ECSS-based scheme achieves a twofold resolution improvement in lossless environments. This quantum enhancement originates from two fundamental mechanisms: first, PD's inherent property of projecting the output state onto a compressed state with an odd or even number of photons, which inevitably improves the resolution of the detected signals; second, the ECSS's coherent superposition characteristic that induces a doubled phase shift, di-

rectly enabling the observed doubled super-resolution. These combined effects explain the scheme's simultaneous achievement of narrow-peak super-resolution and twofold resolution enhancement while maintaining SNL sensitivity.

References

[1] Hu Y, Lv J and Hao Q 2021 *Sensors* **21** 2421
[2] Liu X, Qiaohan W and Wang D 2022 *Optik* **254** 168642
[3] Singh S, Sharma A K, Lohia P, Dwivedi D, Kumar V and Singh P K 2023 *Phys. Scr.* **98** 025813
[4] Rahad R, Rakib A, Haque M A, Sharar S S and Sagor R H 2023 *Results Phys.* **49** 106478
[5] Tuaimah A M, Taher H J, Tahhan S R, Al-Zahrani F A and Ahmed K 2023 *Plasmonics* **18** 2393
[6] Liu Y, Zhang W, Tong Z, Wang X, Liu D, Wang M and Yu H 2024 *Opt. Mater.* **148** 114933
[7] Wu Y, Liu B, Wang J, Wu J, Mao Y, Ren J, Zhao L, Sun T, Nan T and Han Y 2021 *Optik* **226** 165495
[8] Upadhyay C and Dhawan D 2023 *Opt. Quantum Electron.* **55** 271
[9] Guo X, Li C and Cong J 2022 *Optik* **271** 170030
[10] Li K, Guo Y, Li S, Yin Z, Chen Q, Meng X, Gao Z and Bai G 2023 *Plasmonics* **18** 1093
[11] Chen P, Shu X and Cao H 2017 *IEEE Photonics J.* **9** 1
[12] Li X, Warren-Smith S C, Xie L, Ebendorff-Heidepriem H and Nguyen L V 2020 *IEEE Sens. J.* **20** 6408
[13] Zheng S, Rao W, Cai X, Wu M, Xie T and Wang H 2024 *IEEE Photonics J.* **24** 2799
[14] Wang J, Liu B, Wu Y, Mao Y, Zhao L, Sun T and Nan T 2019 *Optik* **194** 163094
[15] Zhao N, Wang Z, Zhang Z, Lin Q, Yao K, Zhu L, Tian B, Zhao L, Yang P and Jiang Z 2022 *Micromachines* **13** 658
[16] Qi K, Zhang Y, Sun J and Yi G 2020 *Opt. Laser Technol.* **129** 106300
[17] Zhang J, Li Y and Yao G 2023 *Int. J. Optomechatronics* **17** 2182389
[18] Ma Y, Yi Y, Li X, Su C, Zhang M, Geng T, Sun W and Yuan L 2021 *Opt. Express* **29** 31443
[19] Jin B, Wang D, Xu B, Chen L and Yang K 2023 *Opt. Fiber Technol.* **80** 103427
[20] Li Y, Chen H, Zhang Y, Chen Q, Wu B, Fan X, Liu Y and Ma M 2023 *Chin. Phys. B* **32** 054209
[21] Cheng J, Wang C, Li Y, Zhang Y, Liu S and Dong P 2024 *Chin. Phys. B* **33** 084201
[22] Hussain N, Masuk M R, Hossain M F and Kouzani A Z 2023 *Opt. Express* **31** 26910
[23] Wang Q and Wang D 2024 *Opt. Fiber Technol.* **83** 103683
[24] Qi Q, Li Y, Liu T, Zhang P, Dai S and Xu T 2023 *Chin. Phys. B* **32** 014204
[25] Dowling J P 2008 *Contemp. Phys.* **49** 125
[26] Boixo S, Datta A, Davis M J, Flammia S T, Shaji A and Caves C M 2008 *Phys. Rev. Lett.* **101** 040403
[27] Boto A N, Kok P, Abrams D S, Braunstein S L, Williams C P and Dowling J P 2000 *Phys. Rev. Lett.* **85** 2733
[28] Qiang W, Qian W, Zhen W and Hao L 2023 *Chin. Opt.* **16** 434
[29] Bollinger J J, Itano W M, Wineland D J and Heinzen D J 1996 *Phys. Rev. A* **54** R4649
[30] Gerry C C 2000 *Phys. Rev. A* **61** 043811
[31] Gerry C C and Mimih J 2010 *Contemp. Phys.* **51** 497
[32] Zhang Z, Qiao T, Ma K, Zhang J, Cen L, Wang F and Zhao Y 2016 *Opt. Express* **24** 18477
[33] Sajeev D, Shaik A, Pidishety S and Soorat R 2024 *J. Quantum Comput.* **6** 53
[34] Zhang Z, Qiao T, Song J, Cen L, Zhang J, Li S, Yan L, Wang F and Zhao Y 2017 *Opt. Commun.* **403** 92
[35] Zhang J, Zhang Z, Cen L, Li S, Zhao Y and Wang F 2017 *Chin. Phys. B* **26** 094204
[36] Huver S D, Wildfeuer C F and Dowling J P 2008 *Phys. Rev. A* **78** 063828
[37] Anisimov P M, Raterman G M, Chiruvelli A, Plick W N, Huver S D, Lee H and Dowling J P 2010 *Phys. Rev. Lett.* **104** 103602
[38] Distante E, Ježek M and Andersen U L 2013 *Phys. Rev. Lett.* **111** 033603
[39] Gerry C C 1993 *J. Mod. Opt.* **40** 1053
[40] Roy Bardhan B, Jiang K and Dowling J P 2013 *Phys. Rev. A* **88** 023857
[41] Cohen L, Istrati D, Dovrat L and Eisenberg H 2014 *Opt. Express* **22** 11945
[42] Podoshvedov S A 2012 *Opt. Commun.* **285** 3896
[43] Dakna M, Anhut T, Opatrný T, Knöll L and Welsch D G 1997 *Phys. Rev. A* **55** 3184
[44] Huang K, Le Jeannic H, Ruaudel J, Verma V B, Shaw M D, Marsili F, Nam S W, Wu E, Zeng H and Jeong Y C 2015 *Phys. Rev. Lett.* **115** 023602
[45] Stammer P, Rivera-Dean J, Lamprou T, Pisanty E, Ciappina M F, Tzallas P and Lewenstein M 2022 *Phys. Rev. Lett.* **128** 123603
[46] Zhu D, Zhao Q Y, Choi H, Lu T J, Dane A E, Englund D and Berggren K K 2018 *Nat. Nanotechnol.* **13** 596
[47] Mattioli F, Zhou Z, Gaggero A, Gaudio R, Jahanmirinejad S, Sahin D, Marsili F, Leoni R and Fiore A 2015 *Supercond. Sci. Technol.* **28** 104001